

Influence of the Francis Turbine location under vortex rope excitation on the Hydraulic System Stability

S. Alligné¹, C. Nicolet², P. Allenbach³, B. Kawkabani³, J.-J. Simond³ and F. Avellan¹

¹Laboratory for Hydraulic Machines, EPFL University
33b. av de Cour, Lausanne, CH-1007, Switzerland

²Power vision engineering sàrl
Chemin des champs, Ecublens, CH-1024, Switzerland

³Laboratory for Electrical Machines, EPFL University
Lausanne, CH-1015, Switzerland

Abstract

Hydroelectric power plants are known for their ability to cover variations of the consumption in electrical power networks. In order to follow this changing demand, hydraulic machines are subject to off-design operation. In that case, the swirling flow leaving the runner of a Francis turbine may act under given conditions as an excitation source for the whole hydraulic system. In high load operating conditions, vortex rope behaves as an internal energy source which leads to the self excitation of the system.

The aim of this paper is to identify the influence of the full load excitation source location with respect to the eigenmodes shapes on the system stability. For this, a new eigenanalysis tool, based on eigenvalues and eigenvectors computation of the nonlinear set of differential equations in SIMSEN, has been developed. First the modal analysis method and linearization of the set of the nonlinear differential equations are fully described. Then, nonlinear hydro-acoustic models of hydraulic components based on electrical equivalent schemes are presented and linearized. Finally, a hydro-acoustic SIMSEN model of a simple hydraulic power plant, is used to apply the modal analysis and to show the influence of the turbine location on system stability. Through this case study, it brings out that modeling of the pipe viscoelastic damping is decisive to find out stability limits and unstable eigenfrequencies.

Keywords: Instability, Vortex rope, Eigenvalues, Viscoelastic damping, Francis Turbine

1. Introduction

At full load operating conditions, Francis turbines feature an axisymmetric cavitation vortex rope in the draft tube cone generated by the incoming swirling flow, see Jacob [1]. The rope may under certain conditions act as an energy source, which leads to self-excited pressure oscillations in the whole hydraulic system [1], [2]. These pressure oscillations can jeopardize the safety of mechanical and hydraulic systems on the prototype, see Jacob 1992 [3].

Koutnik and Pulpitel [4] applied to Francis turbines the modeling approach developed initially for pump stability analysis based on the use of the cavitation compliance C and of the mass flow gain factor χ parameters, see Brennen and Acosta in 1973 [5] and 1976 [6]. Using the transfer matrix method, Koutnik and Pulpitel [4] derived a stability diagram to explain a full load surge occurring on a four 39MW Francis Turbine power plant. A similar approach based on cavitation parameters mapping was also successfully applied to explain inducer instabilities by Tsujimoto et al. in 1993 [7] and propeller instabilities by Duttweiler and Brennen in 2002 [8] and by Watanabe and Brennen in 2003 [9]. In 2006, Koutnik et al. [10], used both transfer matrix method and time domain simulation with SIMSEN software to analyze and quantify a self excited phenomena occurring in a four 400MW Francis Pumped Storage plant. Finally, in 2007 Chen et al. [11] performed a one dimensional stability analysis of a simple hydraulic power plant and showed the destabilizing effect of the diffuser and the swirling flow on the system stability.

The aim of this paper is to identify the influence of the full load excitation source location with respect to the eigenmodes shapes on the system stability. For this purpose, a new eigenanalysis tool, based on eigenvalues and eigenvectors computation of the nonlinear set of differential equations has been developed and implemented in SIMSEN software. First the modal analysis

method and linearization of the set of the nonlinear differential equations in SIMSEN are fully described. Then, nonlinear hydro-acoustic models of hydraulic components based on electrical equivalent schemes are presented and linearized. Finally, a hydro-acoustic SIMSEN model of a simplified hydraulic power plant, is used to apply the new modal analysis and to show the influence of the turbine location on system stability.

2. Modal analysis

2.1 General state space equation

Initially, SIMSEN software was developed by the EPFL for the transient and steady-state simulation of electrical power systems and control devices having an arbitrary topology. Then, the capability of the software was extended to hydraulic components in order to be able to simulate the transient behavior of a complete hydroelectric power plant. The most common hydraulic components have been implemented such as pump-turbine, penstock, surge tank, gallery, valve, reservoir, etc. In order to get a common set of differential equations for both electrical and hydraulic parts, hydraulic models are based on the electrical analogy [12]. Therefore, dynamic behavior of a hydroelectric system, is given by a set of n first order nonlinear ordinary differential equations of the following form:

$$[A] \cdot \frac{d\vec{X}}{dt} + [B(\vec{X})] \cdot \vec{X} = \vec{V}(\vec{X}) \quad (1)$$

where $[A]$ and $[B(\vec{X})]$ are the state global matrices of dimension $[n \times n]$, \vec{X} and $\vec{V}(\vec{X})$ are respectively the state vector and the boundary conditions vector with n components. This set of equations feature nonlinearity since the matrix $[B(\vec{X})]$ and the boundary conditions vector $\vec{V}(\vec{X})$ are function of the state vector.

2.2 Linearization and stabilization assessment

Stability analysis of a hydroelectric system subjected to small perturbations is based on linearization of the nonlinear set of differential equations (1) around an equilibrium point, see [13]. Then, stability is deduced from the eigenvalues of the linearized set of differential equations. Assuming $\vec{f} = [B(\vec{X})] \cdot \vec{X} - \vec{V}(\vec{X})$ a vector of n nonlinear functions, eq. (1) becomes:

$$[A] \cdot \frac{d\vec{X}}{dt} + \vec{f}(\vec{X}) = \vec{0} \quad (2)$$

Considering a small perturbation from the equilibrium point \vec{X}_0 defined by:

$$\vec{X} = \vec{X}_0 + \delta\vec{X} \quad (3)$$

this new state vector must satisfy eq. (1), and using a first order Taylor development it yields to the linearized matrix form:

$$[A] \cdot \frac{d \cdot \delta\vec{X}}{dt} + [B_l] \cdot \delta\vec{X} = \vec{0} \quad (4)$$

with $B_{lij} = \left. \frac{\partial f_i}{\partial X_j} \right|_0$ the linearized state global matrix.

Hence, eigenvalues of the matrix $[M] = -[A]^{-1} [B_l]$ define the sytem stability. They can be either real or complex numbers. A real eigenvalue is a non oscillatory eigenmode whereas a complex eigenvalue is an oscillatory one. In both cases damping and oscillation frequency of the eigenmode are respectively given by the real part and the imaginary part of the eigenvalue. Therefore, if at least one of the eigenvalue has a positive real part, the system is unstable.

3. Modeling and linearization of hydraulic components

The aim of this paper is to show the influence on the system stability, of the vortex rope location with respect to the eigenmodes shapes of the hydraulic system. Hence, the modal analysis is applied to a simple hydraulic power plant including viscoelastic pipes and a Francis turbine with a cavitation vortex rope. Nonlinear models of hydraulic elements involved in this case study are presented and linearized in this section.

3.1 Viscoelastic Pipe

By assuming uniform pressure and velocity distributions in the cross section and neglecting the convective terms, the one-dimensional momentum and continuity balances for an elementary pipe filled with water of length dx , cross section A and wave

speed a , yields to the well known Allievi hyperbolic equations, see [14], [15]. Using the Finite Difference Method with a 1st order centered scheme discretization in space and a scheme of Lax for the discharge variable, this approach leads to a set of ordinary differential equations (1) which can be represented as a T-shaped equivalent electrical scheme shown in Fig. 1. The RLC parameters of this equivalent scheme are given by:

$$R_i = \frac{\lambda |Q_i| dx}{2gDA^2}; L = \frac{dx}{gA}; C = \frac{gAdx}{a^2} \quad (5)$$

where λ is the local loss coefficient. The hydraulic resistance R , the hydraulic inductance L , and the hydraulic capacitance C correspond respectively to energy losses, inertia and storage effects due to wall deflection and fluid compressibility. Moreover, in order to predict accurately pressure fluctuation amplitudes and system stability, it is necessary to take into account the viscoelastic behavior due to an energy dissipation during the wall deflection. This additional dissipation leads to a resistance in series with the capacitance as shown in Fig. 1.

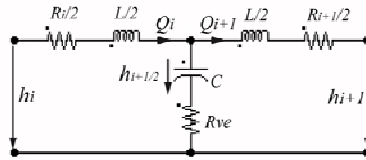


Fig. 1 Electrical equivalent scheme of a pipe of length dx with viscoelastic resistance

This viscoelastic resistance is accounting for both fluid and pipe material viscoelasticity and can be expressed as:

$$R_{ve} = \frac{\mu_{equ}}{A \cdot \rho \cdot g \cdot dx} \quad (6)$$

with μ_{equ} the equivalent viscoelastic damping of both the fluid and the wall. The resulting set of nonlinear differential equations relative to the equivalent electrical circuit is set up using Kirchoff laws and can be written under matrix form:

$$\begin{bmatrix} C & 0 & 0 \\ 0 & L/2 & 0 \\ 0 & 0 & L/2 \end{bmatrix} \cdot \frac{d}{dt} \begin{pmatrix} h_{i+1/2} \\ Q_i \\ Q_{i+1} \end{pmatrix} + \begin{bmatrix} 0 & -1 & 1 \\ 1 & R_i/2 + R_{ve} & -R_{ve} \\ -1 & -R_{ve} & R_{i+1}/2 + R_{ve} \end{bmatrix} \cdot \begin{pmatrix} h_{i+1/2} \\ Q_i \\ Q_{i+1} \end{pmatrix} = \begin{pmatrix} 0 \\ h_i \\ -h_{i+1} \end{pmatrix} \quad (7)$$

Resistance R_i , proportional to the discharge Q_i , induces a nonlinearity proportional to the square exponent of the discharge. Applying the linearization, it yields to:

$$\delta(R_i \cdot Q_i^2) = 2 \cdot R_i' \cdot Q_i|_0 \cdot \delta Q_i \quad (8)$$

where $Q_i|_0$ is the discharge at the equilibrium point and R_i' the reduced resistance defined by:

$$R_i' = \frac{\lambda \cdot dx}{2gDA^2} \quad (9)$$

Hence, the linearized state global matrix for the viscoelastic pipe is:

$$[B_l]_{\text{viscoelastic pipe}} = \begin{bmatrix} 0 & -1 & 1 \\ 1 & R_i' \cdot Q_i|_0 + R_{ve} & -R_{ve} \\ -1 & -R_{ve} & R_{i+1}' \cdot Q_{i+1}|_0 + R_{ve} \end{bmatrix} \quad (10)$$

3.2 Francis Turbine

Francis turbine can be modeled as a pressure source converting hydraulic energy into mechanical work, an inductance related to the inertia effects of the water and a resistance which models the head losses through the turbine. The resulting nonlinear differential equation is:

$$L_t \frac{dQ_i}{dt} + R_t Q_i = -H_t + H_i - H_{\bar{t}} \quad (11)$$

Moreover, momentum equation applied to the rotational inertias is taken into account and leads to:

$$J_t \cdot \frac{d\omega}{dt} = T_t - T_{elec} \quad (12)$$

where J_t , ω , T_t , T_{elec} are respectively turbine inertia, rotational speed, mechanical torque and electromagnetic torque.

Combined with eq. (11) the set of differential equations under matrix form is:

$$\begin{bmatrix} L_t & 0 \\ 0 & J_t \end{bmatrix} \cdot \frac{d}{dt} \begin{pmatrix} Q_i \\ \omega \end{pmatrix} + \begin{bmatrix} R_t & 0 \\ 0 & 0 \end{bmatrix} \begin{pmatrix} Q_i \\ \omega \end{pmatrix} = \begin{pmatrix} -H_t + H_l - H_{\bar{l}} \\ T_t - T_{elec} \end{pmatrix} \quad (13)$$

The pressure source $H_t(Q_i, \omega, y)$ and the mechanical torque $T_t(Q_i, \omega, y)$ are driven by the turbine characteristics which are nonlinear functions of the discharge, the rotational speed and the guide vane opening. In the same way as the viscoelastic pipe model, the resistance term of the Francis Turbine model induces a nonlinearity proportional to the square exponent of the discharge. Therefore the linearization of this term is identical. On the other part, the linearization of the pressure source and the mechanical torque is given by [16]:

$$\delta H_t = \left. \frac{\partial H_t}{\partial Q_i} \right|_0 \cdot \delta Q_i + \left. \frac{\partial H_t}{\partial \omega} \right|_0 \cdot \delta \omega + \left. \frac{\partial H_t}{\partial y} \right|_0 \cdot \delta y \quad (14)$$

$$\delta T_t = \left. \frac{\partial T_t}{\partial Q_i} \right|_0 \cdot \delta Q_i + \left. \frac{\partial T_t}{\partial \omega} \right|_0 \cdot \delta \omega + \left. \frac{\partial T_t}{\partial y} \right|_0 \cdot \delta y \quad (15)$$

where partial derivative terms are the gradients of the characteristic curves at the equilibrium point. Hence, the linearized state global matrix is:

$$[B_l]_{\text{turbine}} = \begin{bmatrix} 2R_{t_0} + \left. \frac{\partial H_t}{\partial Q_i} \right|_0 & \left. \frac{\partial H_t}{\partial \omega} \right|_0 \\ \left. \frac{\partial T_t}{\partial Q_i} \right|_0 & \left. \frac{\partial T_t}{\partial \omega} \right|_0 \end{bmatrix} \quad (16)$$

3.3 Pipe with Vortex rope self excitation

Gaseous volume of a vortex rope at full load conditions can be modeled as a function of two state variables: the head and the discharge [5], [6]. Therefore the resulting state space continuity equation defining the discharge variation due to the occurrence of gaseous volume at the node $i + 1/2$ is:

$$Q_i - Q_{i+1} = C_{\text{rope}} \frac{dH_{i+1/2}}{dt} + \chi \frac{dQ_{i+1}}{dt} \quad (17)$$

where C_{rope} and χ are respectively the rope cavitation compliance and the mass flow gain factor defined by:

$$C_{\text{rope}} = -\frac{\partial V_{\text{rope}}}{\partial H_{i+1/2}}; \chi = -\frac{\partial V_{\text{rope}}}{\partial Q_{i+1}} \quad (18)$$

The resulting equivalent electrical scheme of a vortex rope at full load conditions is given in Fig. 2 a).

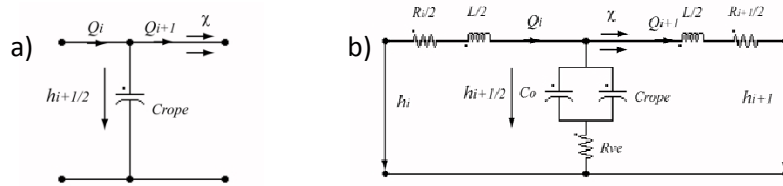


Fig. 2 a) Vortex rope modeling b) Pipe of length L with vortex rope self excitation

Modeling of a pipe of length l with a vortex rope self excitation, implies to combine the equivalent electrical schemes of the vortex rope and the viscoelastic pipe. Moreover, only one pressure node is used to model the pipe of length l , see Fig. 2 b). It leads to an equivalent concentrated compliance C_{equ} defined by two capacitances in parallel:

$$C_{\text{equ}} = C_0 + C_{\text{rope}} \quad (19)$$

where C_0 is the compliance of the wall deformation. Hence, to model the vortex rope self-excitation in pipe, two rope parameters are available: the rope cavitation compliance and the mass flow gain factor. For this investigation, cavitation rope compliance and mass flow gain factor are constant. Therefore nonlinearity and linearization are the same as the ones of the viscoelastic pipe model.

4. Case studies

Power and pressure fluctuations have been experienced at full load operating conditions during commissioning tests in a Pumped-Storage plant located in the southeastern United States featuring four 400MW Francis pump-turbines [10]. Koutnik et al. showed that the cavitation compliance and the mass flow gain factor of the vortex rope, reached unstable values because of the shutdown of one pump turbine. The aim of this paper is to highlight that unstable rope parameters can be stable for another location in the hydraulic system. This analysis shows the influence on the stability of the vortex rope location with respect to the eigenmodes shapes of the hydraulic system. First a simple case including a pipe with cavitation development is treated and results are used to analyze the instability of a simple hydraulic power plant.

4.1 Pipe with cavitation development

The first case study is a pipe with uniform cross section subdivided in three parts as illustrated in Fig. 3. The central part is where the cavitation development is modeled with the vortex rope self excitation model, see Fig. 2 b). Hence, the self-excitation can be located everywhere along the pipe adjusting the lengths of the upstream and the downstream pipes.

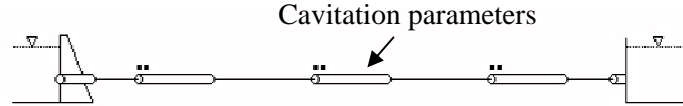


Fig. 3 Pipe with cavitation development

Both viscoelastic damping and location of the excitation, influence the stability limits of the system. First of all, to predict accurately stability limits and amplitude of pressure fluctuations, the equivalent viscoelastic damping parameter μ_{equ} of the pipe model is decisive. To assess the effect of this parameter, cavitation development is not taken into account in the system by putting compliance and mass flow gain factor equal to zero. System eigenvalues are computed for different equivalent viscoelastic dampings and plotted in Fig. 4 a). Moreover, for the first ten eigenmodes, damping is plotted as function of the equivalent viscoelastic damping in Fig. 4 b).

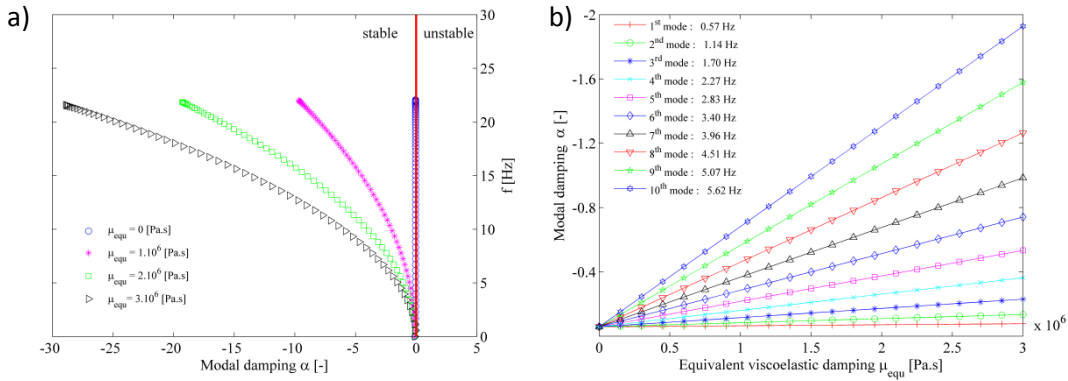


Fig. 4 Influence of the viscoelastic damping on eigenvalues

If the viscoelastic damping is equal to zero, then damping of all the eigenmodes are equal. However, according to the Fig. 4 b), the more the viscoelastic damping is high, the more the modal damping increases. Moreover, for a given viscoelastic damping, eigenmodes of high frequencies have a damping higher than low frequencies. Therefore, this parameter introduces a frequency-dependent damping of the system as [17].

Then, influence on stability of the self-excitation location is investigated. Fig. 5 shows the first six eigenmodes computed for the system without cavitation. The effect of two excitation locations are studied and are symbolized in Fig. 5 by the vertical dashed lines:

$$\frac{x_{excitation}}{l} = 0.5 \text{ or } 0.75.$$

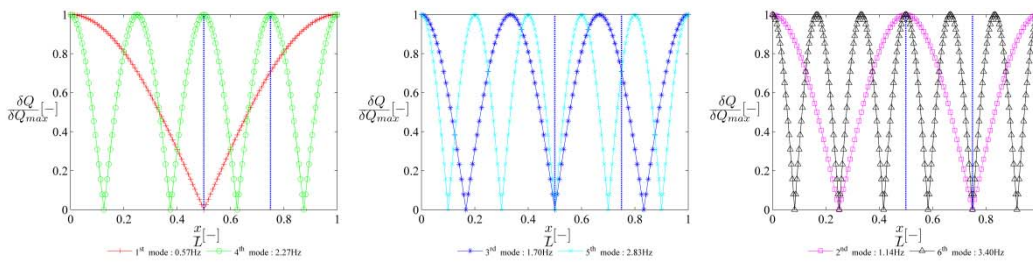


Fig. 5 Discharge modes of a uniform pipe without cavitation development

Taking into account the cavitation parameters, eigenvalues are computed for these two locations and are compared to the eigenvalues of the system without cavitation, see Fig. 6. Abscissa is the eigenvalue real part i.e. the modal damping and the ordinate is the imaginary part i.e. the frequency. Fig. 6 a) is given for the system without viscoelastic damping and Fig. 6 b) for a viscoelastic damping of $\mu_{equ} = 3.10^6$ Pa.s .

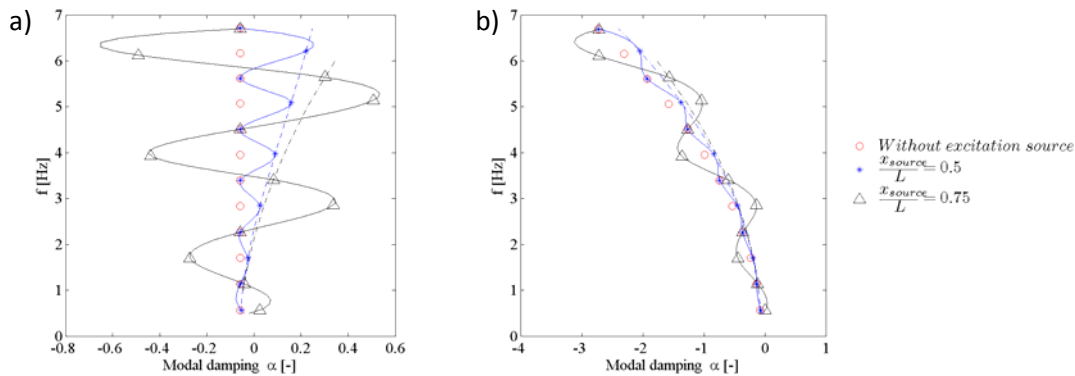


Fig. 6 Influence of excitation location on modal dampings (a) without and (b) with viscoelastic damping

For a given location of the excitation source, two kinds of eigenmodes must be identified: the ones which excitation is located on a discharge node, showed by the dashed lines in Fig. 6, and the others. For instance, when excitation is located at the half of the pipe length, odd eigenmodes are excited on a node whereas three quarter of the pipe length corresponds to a node only for the 2nd, 6th and 10th eigenmodes. In such situation, the modal damping of the excited eigenmode is increased. The more the eigenmode is high, the more the increase of the damping is significant, see the shape of the dashed lines in Fig. 6. For the remaining eigenmodes where excitation is not located on a node, the modification of the modal damping depends on the sign of the eigenmode slope. When the latter is positive, the damping increases whereas it decreases when the sign is negative, see respectively 3rd and 5th eigenmode for an excitation at three quarter of the pipe length. The higher is the slope, the higher the modification of the damping is significant. When the slope is equal to zero on an antinode, the damping is unchanged. One can observe, that influence of excitation is more important in this situation than in the particular case of a location on a node. Instability occurs when a modal damping is increased and becomes positive. Therefore, according to the previous observations, the most critical location of the excitation is not on a node but where the slope is positive and maximum. In the case of a system without viscoelastic damping, see Fig. 6 a), the most unstable eigenmode has a high frequency, since its slope is the highest. However if a viscoelastic damping is taken into account, see Fig. 6 b), the same behaviors are observed but eigenmodes with high frequency are damped and therefore become stable. Hence, potential unstable eigenmodes should have a low frequency.

4.2. Hydraulic power plant

The simplified hydraulic power plant features two significant pipe cross sections as illustrated in Fig. 7 and mentioned in Tab. 1. From this simple installation, a one dimensional hydroacoustic model is carried out. Full load operating conditions defined in Tab. 1 are investigated with the modal analysis to show the influence of the vortex rope self-excitation location on system stability.

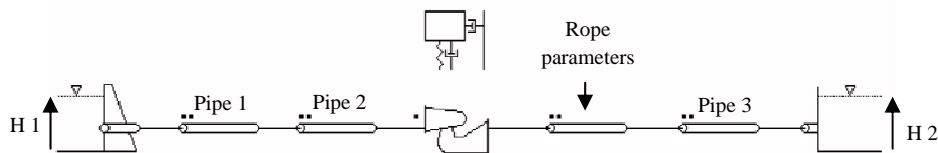


Fig. 7 Simplified layout

Table 1 Layout dimensions and turbine parameters

Reservoirs		Pipe 1		Pipe 2		Pipe 3		Pump turbine	
H1	497 m	I1	615 m	I2	180 m	I3	85 m	Specific speed	0.306
H2	194 m	D1	10 m	D2	5 m	D3	5 m	Nominal rotational speed	300 rpm
		a1	1 000 m/s	a2	1 200 m/s	a3	1 200 m/s	Moment of inertia	$2.77 \cdot 10^6$ kg.m ²
								Thoma number	0.18

l_i , D_i and a_i are respectively length, diameter and wave speed of the i^{th} pipe. System stability is assessed by computing eigenvalues as function of the two rope parameters in Fig. 8 a). Eigenvalues with positive real part are plotted which allows to identify unstable couple parameters. For this investigation, the chosen rope parameters are: $C = 0.01 \text{ m}^2$ and $\chi = -0.04 \text{ s}$. According to the instability diagram of Fig. 8 a), these parameters are identified as unstable ones, leading to eigenvalues plotted in Fig. 8 b).

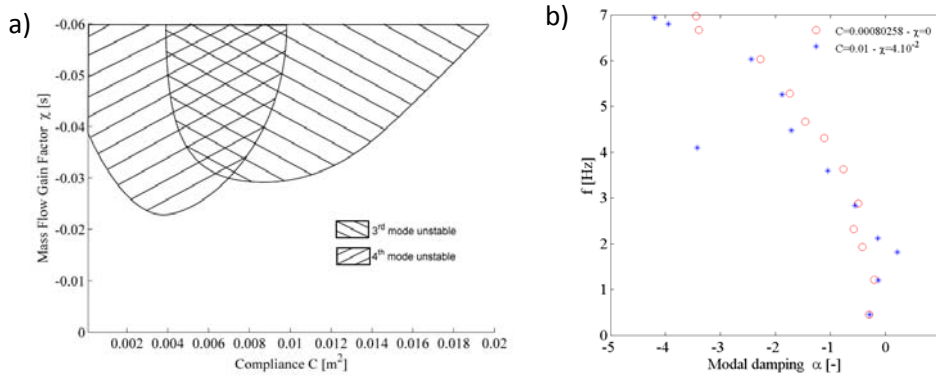


Fig. 8 (a) Instability diagram (b) Eigenvalues for unstable rope parameters

In this configuration, the third eigenmode, which frequency is 1.8 Hz, is unstable. In order to explain why the third eigenmode damping is positive, conclusions established from the case study of the uniform pipe with cavitation development, can be used. In Fig. 9, the first discharge modes are plotted a) without and b) with rope self-excitation. The two vertical dashed lines located at $\frac{x}{l} = 0.7$ and $\frac{x}{l} = 0.9$ symbolize respectively the change of the pipe cross section and the location of the turbine. At this turbine position, the first and the second eigenmodes have slight positive slopes. Therefore, dampings are slightly increased but not sufficient to become positive. Then according to the third and the fourth eigenmodes, excitation is located on a significant positive slope, inducing an increase of the dampings. However, viscoelastic damping reduces more the increase of the fourth eigenmode than the third one, which explains why it is only the third eigenmode which becomes unstable.

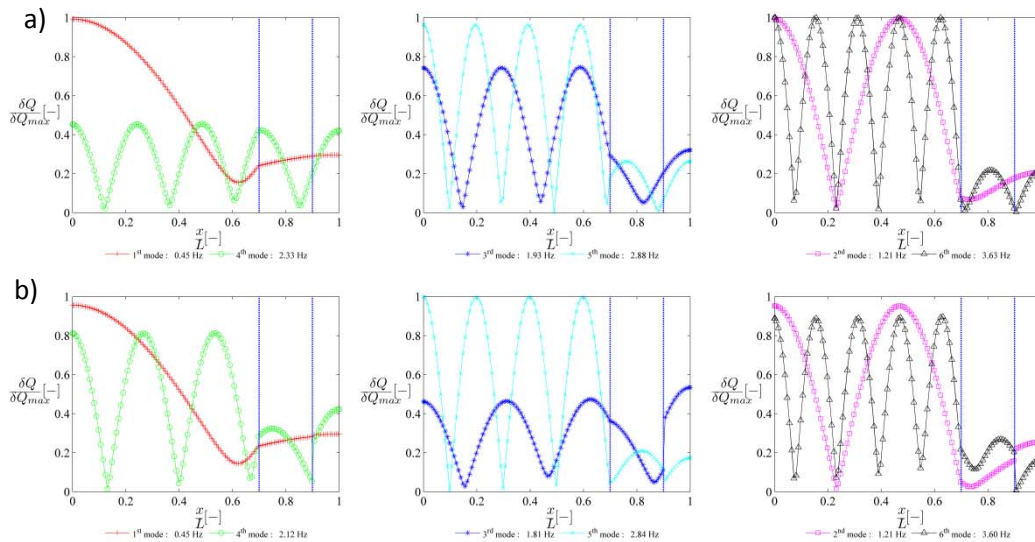


Fig. 9 Discharge modes (a) without rope excitation and (b) with rope excitation

Turbine location is now considered as a parameter. The aim is to identify if for these unstable rope parameters, a stable location exists or not. Therefore, system eigenvalues have been computed for different locations between the cross section change and the downstream reservoir, see Fig. 10. Modal damping and frequency evolution of the first eigenmodes are plotted as function of the turbine location.

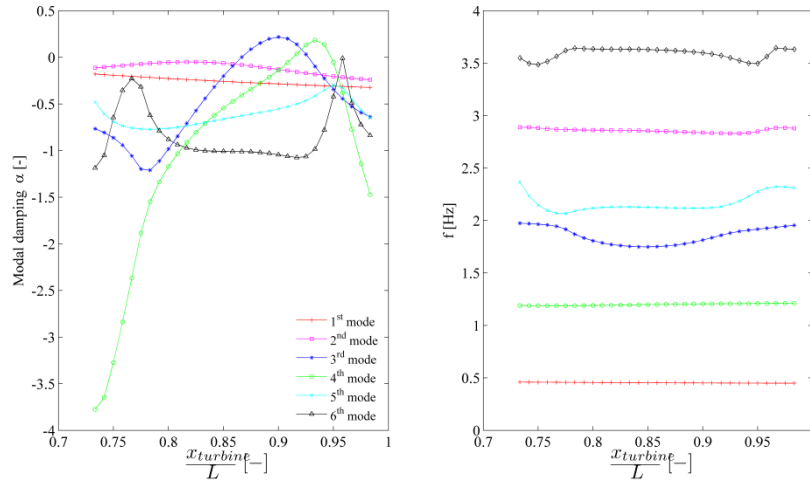


Fig. 10 Turbine position effect on eigenvalues

Only the third and the fourth eigenmodes feature positive modal damping which may appear if the turbine is located between $\frac{x_{turbine}}{l} = 0.86$ and $\frac{x_{turbine}}{l} = 0.95$. Therefore if the turbine is out of this area which corresponds to 79 m length, the system is stable for the given rope parameters.

5. Conclusion

Modal analysis based on eigenvalues and eigenmodes computation of the set of nonlinear differential equations has been introduced and used to assess influence of turbine location on the system stability at full load conditions. It has been showed that relative position of the excitation with respect to the eigenmode shapes, changes the eigenmode dampings. Moreover, modeling of the viscoelastic behavior induces a frequency dependent damping which is more significant for high frequencies. Therefore, the worst location for a full load self-excitation is where the maximum positive slope of a low discharge eigenmode is observed. With such an analysis, the relative location of the turbine can be optimized at early stage of hydroelectric project for stability assessment.

Acknowledgments

This study is carried out in the framework of the project financially supported by Alstom Power Hydro and CTI the Swiss Federal Commission for Technology and Innovation, grant CTI n° 8330-2. The authors took advantages of the development of the SIMSEN hydraulic extension, developed in collaboration with the EPFL Laboratory for Electrical Machines.

Nomenclature

l	Loss coefficient [-]	Q	Discharge [$\text{m}^3 \cdot \text{s}^{-1}$]
g	Gravity acceleration [$\text{m} \cdot \text{s}^{-2}$]	H	Pressure [m]
D	Diameter, [m]	c	Mass flow gain factor [s]
ρ	Fluid density, [$\text{kg} \cdot \text{m}^{-3}$]	C_{rope}	Rope compliance [m^2]
A	Cross section, [m^2]	a	Wave speed [$\text{m} \cdot \text{s}^{-1}$]
R	Resistance, [$\text{s} \cdot \text{m}^{-2}$]	m_{equ}	Equivalent viscoelastic damping [Pa.s]
L	Inductance, [$\text{s}^2 \cdot \text{m}^{-2}$]	α	Modal damping [-]
C	Capacitance, [m^2]	f	Frequency [Hz]
R_{ve}	Viscoelastic resistance, [$\text{s} \cdot \text{m}^{-2}$]	w	Rotational frequency [Hz]
l	Length [m]	J_t	Turbine inertia [$\text{kg} \cdot \text{m}^2$]
dx	Elementary length [m]	T_t	Turbine torque [N.m]
y	Guide vane opening [-]	H_t	Turbine head [m]

References

- [1] Jacob, T., 1994, "Similitude in stability of operation tests for Francis turbine," *Hydropower & Dams*, Vol. 1.
- [2] Jacob, T., Prénat, J.E. and Maria, D., 1988, "Comportement dynamique d'une turbine Francis à forte charge comparaison modèle prototype", *La houille blanche*, Vol. 3, pp. 293-300.
- [3] Jacob, T., Prénat, J.E., Vullioud, G. and Araguas, B.L., 1992, "Surging of 140MW Francis Turbine at high load, analysis and solution," *IAHR Symposium on Hydraulic Machinery and systems*, Sao Paolo.
- [4] Koutnik, J. and Pulpitel, L., 1996, "Modelling of the Francis Turbine full load surge," *IAHR Symposium on Hydraulic Machinery and systems*, Lausanne.
- [5] Brennen, C. and Acosta, A.J., 1973, "Theoretical, quasi static analysis of cavitation compliance in turbopumps," *Journal Spacecraft*, Vol. 10, pp. 175-180.
- [6] Brennen, C. and Acosta, A.J., 1976, "The dynamic transfer function for a cavitating inducer," *Journal of fluids engineering ASME*, Vol. 98, pp. 182-191.
- [7] Tsujimoto, Y., Kamijo, K. and Yoshida, Y., 1993, "Theoretical analysis of rotating cavitation in inducers," *Journal of fluids engineering ASME*, Vol. 115, pp. 135-141.
- [8] Duttweiler, M. and Brennen, C., 2002, "Surge instability on a cavitating propeller," *Journal of fluids Mechanics*, Vol. 458, pp. 133-152.
- [9] Brennen, C. and Watanabe, S., 2003, "Dynamics of a cavitating propeller in a water tunnel," *Journal of fluids engineering*, Vol. 125, pp. 283-292.
- [10] Koutnik, J., Nicolet, C., Schohl, G.A. and Avellan, F., 2006, "Overload surge event in a pumped storage power plant," *IAHR Symposium on Hydraulic Machinery and systems*, Yokohama.
- [11] Chen, C., Nicolet, C., Yonezawa, K., Farhat, M., Avellan, F. and Tsujimoto, Y., 2007, "One dimensional analysis of full load draft tube surge," *ASME fluids engineering*, San Diego.
- [12] Nicolet, C., Greiveldinger, B., Herou, J.J., Kawkabani, B., Allenbach, P., Simond, J.J. and Avellan, F., 2007, "High order modeling of Hydraulic Power Plant in Islanded Power Network," *IEEE Transactions of powersystem*, Vol 22.
- [13] Kundur, P., 1994, "Power system stability and control," EPRI.
- [14] Nicolet, C., 2007, "Hydroacoustic modelling and numerical simulation of unsteady operation of hydroelectric systems," Ph. D. Thesis N°3751, Laboratory for Hydraulic Machines, Swiss Federal Institute University, Lausanne.
- [15] Wylie, B. and Streeter, V., 1993, "Fluid transients in systems," E.C Prentice Hall, New Jersey.
- [16] Xianlin, L. and Chu, L., 2007, "Eigenanalysis of Oscillatory Instability of a Hydropower Plant Including Water Conduit Dynamics," *IEEE Transactions on Power Systems*, Vol 22 (2), pp. 675-681
- [17] Haban, V., Koutnik, J. and Pochyly, F., 2002, "1D mathematical model of high frequency pressure oscillations induced by RSI including an influence of fluid second viscosity," *IAHR Symposium on Hydraulic Machinery and systems*, Lausanne.